Available online at www.sciencedirect.com
ScienceDirect
Cement and Concrete Research 38 (2008) 616–623
Cement and Concrete Research

Modelling thixotropic behavior of fresh cement pastes from MRI measurements

S. Jarny [a,*], N. Roussel [b], R. Le Roy [c], P. Coussot [d]

[a] Laboratoire d'Études Aérodynamiques (LEA) Université de Poitiers, ENSMA, CNRS, Boulevard Marie et Pierre Curie, Téléport 2, B.P. 30179, 86962 Futuroscope Chasseneuil cedex, France
[b] Division Bétons et Composites Cimentaires, Laboratoire Central des Ponts et Chaussées, 58 boulevard Lefebvre, 75732 Paris cedex 15, France
[c] Laboratoire Analyse des Matériaux et Identification, Institut Navier, 6 et 8 avenue Blaise Pascal, Cité Descartes, Champs sur Marne, 77455 Marne la Vallée cedex 2, France
[d] Université Paris-Est, Institut Navier, 2 allée Kepler, 77420 Champs sur Marne, France

Received 1 February 2007; accepted 8 January 2008

Abstract

From MRI measurements we show that in a flowing cement paste thixotropic effects dominate over short time scales while irreversible effects become significant over larger timescales. The steady and transient flows exhibit a yielding behavior which differs from usual yield stress model: the transition from the solid to the liquid regime is abrupt. We propose a simple thixotropic model based on these observations. The validation is done on the steady and transient state on local experimental tests. We build the "local" rheogram which is representative of the intrinsic rheological properties. Comparisons with "apparent" rheograms demonstrate that it is possible to use correction techniques from the literature to have access to the real behavior law of the material from standard measurements but that, in the case of the material studied in this paper, this would nevertheless lead to an underestimation of the yield stress.

Keywords: Rheology; Cement paste; Thixotropy; Magnetic resonance imaging; Model

1. Introduction

The measurement of rheological properties of cement pastes is based on the use of rheometers and on the measurement of macroscopic values such as torque or rotation speed in steady state flow of the tested material. Models such as Bingham, Herschel–Bulkley, Ellis, Casson or Eyring are then applied to the experimental data in order to obtain fitted values of these models parameters [1,2]. However, this approach often neglects the possible strong heterogeneity of the shear rate distribution within rheometers (parallel plates, coaxial cylinders...). This can significantly affect the apparent behavior of the materials since the effective (local) shear rate in the sample may widely differ from the apparent shear rate estimated, for example, from the measured rotation speed. The access to local values of the shear rate, although difficult from a practical point of view as will be shown in this paper, may allow for a correct identification of the rheological parameters of the tested material.

It has also to be kept in mind that, as shown by Otsubo et al. [3], the flow properties of fresh cement pastes continuously evolve in time. Under fixed boundary conditions (torque or rotation velocity), the apparent viscosity first decreases with time until reaching a minimum and then starts to increase. Banfill and Saunders [4] and Lapasin et al. [5] demonstrated that the first phase is dominated by a de-structuration phenomenon under constant shear rate (thixotropic behavior). Once this phenomenon has reached some equilibrium, the behavior keeps on evolving because of the hydration process.

In the present paper, we present a rheological study of a cement paste carried out with the help of a Couette viscometer

* Corresponding author. Tel.: +33 5 49 49 69 24; fax: +33 5 49 49 69 68.
E-mail addresses: sebastien.jarny@lea.univ-poitiers.fr (S. Jarny), nicolas.roussel@lcpc.fr (N. Roussel), robert.leroy@lami.enpc.fr (R. Le Roy), philippe.coussot@lcpc.fr (P. Coussot).

0008-8846/$ - see front matter © 2008 Elsevier Ltd. All rights reserved.
doi:10.1016/j.cemconres.2008.01.001

inserted in a Magnetic Resonance Imager (MRI) making it possible to measure the local velocity field and thus calculate the local shear rate during transient and steady state flows. Since the local shear stress distribution is well controlled in such a Couette flow, this technique allows for the measurement of the local shear stress and shear rate in the sample and thus gives access to the effective (local) behavior law of the material.

In the first section, the main features of Couette flow viscometers are reviewed and a simple thixotropy model is described. Experimental results obtained from MRI measurements and from standard rheometry tests are then presented and analyzed. It is then shown that classical yield stress models are not able to predict the measured local velocity field whereas the predictions of the simple thixotropy model used here are in good agreement with our measurements. Finally, the local (or real) behavior law of the studied cement paste is deduced from the local MRI measurements and compared to the apparent behavior law calculated from standard rheometric measurements. It is finally demonstrated that it is possible to use correction techniques from the literature to have access to the real behavior law of the material from these standard measurements but that, in the case of the material studied in this paper, this would nevertheless lead to an underestimation of the yield stress.

2. Couette flow and thixotropy model

It may be useful to remember here that, in Couette flow configuration, the shear stress distribution inside the gap is defined by:

$$\tau = \frac{C}{2\pi r^2 h} \tag{1}$$

where C is the applied torque on the inner cylinder, h the height of the inner cylinder and r the local radius varying between the inner and outer cylinders radii. This means that, in the case of a yield stress fluid, there exists a critical radius r_c, corresponding to the position of the interface between the zone where the shear stress is higher than the yield stress τ_c and the zone where the shear stress is lower than the yield stress (*i.e.* sheared and unsheared zones), which is written:

$$r_c = \sqrt{\frac{C}{2\pi h \tau_c}}. \tag{2}$$

The shear rate distribution, in this geometry, is a function of the tangential velocity v_θ:

$$\dot{\gamma} = \left| r \frac{\partial}{\partial r}\left(\frac{v_\theta}{r}\right)\right|. \tag{3}$$

In practice, the shear rate heterogeneities described above are, most of the time, not taken into account and it is often assumed that the gap is entirely sheared. The set of apparent shear rates $\dot{\gamma} = \Omega r_1/(r_2 - r_1)$ and corresponding apparent shear stresses $\tau = C/2\pi h r_1^2$ allows for the identification of the apparent macroscopic behavior law of the tested material (r_1 and r_2 are respectively the radii of the inner and outer cylinder). An alternative method allowing for the consideration of the unsheared zone is the use of the Reiner–Rivlin equation.

However, cementitious materials do not only have a yield stress but they are also thixotropic fluids. Several models in the literature, more or less sophisticated, describe the thixotropic properties of cementitious materials. Tatersall [6] and Papo [7] proposed from their experimental observations very simple thixotropy models which predict an exponential decrease of the shear stress (or torque) if a constant shear rate is applied to the material. Recently, at the other end of the scale of complexity, Wallevik [8] presented a far more sophisticated approach derived from a rather complete physical description of the flocculation and dispersion of the cement grains. He demonstrated that, using these mechanisms, the steady state and transient behavior of fresh cement pastes could be described.

From a more general point of view, the behavior of a thixotropic fluid in nature or industry is necessarily at least represented by an apparent viscosity, *i.e.*$\eta = \tau/\dot{\gamma}$ where τ and $\dot{\gamma}$ are respectively the shear stress and the shear rate magnitudes. This apparent viscosity depends on the extent of structure in the material, or more generally its "degree of jamming" [9,10]. Cheng and Evans [11] suggested a general mathematical form of the equation of state of a thixotropic material, which is written as:

$$\tau = \eta(\lambda, \dot{\gamma})\dot{\gamma} \tag{4}$$

$$\frac{d\lambda}{dt} = f(\lambda, \dot{\gamma}). \tag{5}$$

Eq. (5) is an evolution equation and λ is a structural parameter related to the extent of structure within the material. In addition, it is proposed that the rate of change of λ is equal to the sum of a term expressing the "natural" tendency of the structure in the material to rebuild and a rate of breakdown of structure due to flow, which is proportional to the shear rate and to the instantaneous extent of structure. The model of Coussot et al. [12] uses these simple basic ideas and is written:

$$\tau = \eta_0(1 + \lambda^n)\dot{\gamma} \tag{6}$$

$$\frac{d\lambda}{dt} = \frac{1}{\theta} - \alpha\lambda\dot{\gamma}. \tag{7}$$

where η_0 is the viscosity at infinite shear rate (*i.e.* when λ tends toward zero), n is a constant positive parameter, $1/\theta$ is the characteristic time of structural build-up and α is a dimensionless parameter. The second term in Eq. (7) can be associated with the rate of structural breakdown. This model has been used to model bentonite flows in a Couette viscometer with a large gap [13]. The local predictions of the model were in good agreement with MRI measurements of the local flowing velocities. This model was also applied to macroscopic rheological measurements of cement pastes [14] and, recently, a derivative form of this model, including a yield stress depending on λ, was also applied by Roussel [15] to the steady and transient behavior of fresh concrete.

It may at first sight seem that the above model in its original form (Eqs. (6) and (7)) is not able to describe the yield stress

Table 1
Cement paste composition

Component	Mass [g]
White cement CEM I 52,5 Calcia "Cruas"	2000
Superplasticizer optima 100 Chryso	46.7
Nano silica Rhoximat Rhodia	177
Distilled water	530.3

fluid behavior of most cement pastes as this model does not display an explicit yield stress. However, Roussel et al. [13] have demonstrated that this model includes a critical shear rate, below which flow of the material cannot occur, given by:

$$\dot{\gamma}_c = \frac{k}{\alpha\theta}. \tag{8}$$

where $k=(n-1)^{1/n}$. This critical shear rate is associated with a critical extent of structure $\lambda_c = 1/k$ and a critical shear stress which corresponds implicitly to a yield stress:

$$\tau_c = \tau(\dot{\gamma}_c) = \eta_0\left(\frac{n}{n-1}\right)\dot{\gamma}_c. \tag{9}$$

3. Materials and procedures

3.1. Mix composition

We chose in this work to use white cement instead of classical cement in order to minimize the amount of C_4AF in the material, because Fe paramagnetic oxides in C_4AF enhance the relaxation kinetics, thus leading to very poor signal to noise ratio during MRI measurements. As the cement suspensions studied had to be stable for at least the duration of our tests, a viscosity agent was added to the mixtures. After several preliminary rheometrical tests with various materials, we finally chose the mix composition given in Table 1 which provided us with a cement paste displaying a rheological behavior that was representative of the various tested batches (*i.e.* yield stress and shear thinning behavior, obvious structural build-up at rest and structural breakdown under flow as observed by other authors [16]). The *W/C* ratio of this cement paste was 0.35.

3.2. Preparation procedure

The super-plasticizer was first introduced in the water and the solution obtained was mixed at low speed for 60 s. The white cement and the nano-silica particles were then added. The suspension obtained was mixed at high speed for 15 min and then at low speed for 15 min.

3.3. MRI testing procedures

In the present study, proton NMR velocity measurements were carried out with a Bruker Biospec 24/80 DBX imager located at LMSGC. It was equipped with a 0.5 T vertical magnet (20 MHz proton frequency, diameter: 40 cm), with shielded gradient coils delivering a gradient of 50 mT/m, and with a linear birdcage RF coil (length 24 cm and inner diameter 20 cm). For the purpose of such coupled MRI-rheometry experiments, a home made Couette rheometer was used, specifically designed to comply with MRI constraints. All the parts of the apparatus inserted in the magnet were built with non-magnetic materials and the motor was moved away as far as possible from the magnet entrance. We used a coaxial cylinder viscometer (inner cylinder: $r_1=40.7$ mm (radius), length: $h=113.5$ mm) with a stationary outer cylinder (radius $r_2=59.3$ mm). The surfaces of the outer and inner cylinder in contact with the fluid were covered with sandpaper with an equivalent roughness of 200 μm. The temperature of the material in the Couette geometry could not be controlled but the room temperature was kept between 20° and 24°. A more detailed description of this apparatus can be found in [17].

After a 2 min pre-shearing phase at 134 rpm, the speed of rotation was immediately switched down to a fixed value between 10.3 and 82.4 rpm at which speed it was left for half an hour. Throughout the test, the local velocity field in the sample was measured every 10 s. A new sample was prepared for each test. MRI velocity measurements inside the Couette cell were obtained according to the method first introduced by Hanlon et al. [18] and further modified by Raynaud et al. [19].

3.4. Classical rheometry procedure

Conventional rheometrical tests were also carried out on the same cement paste with a Bohlin C-VOR rheometer equipped with two Couette geometries. The first one was identical to the geometry used in the MRI and will be called "very large gap geometry" in the following (cf. Fig. 1) and the second one had inner radius 12 mm and outer radius 18.2 mm and will be called "large gap geometry". We also carried out tests using a Rheologica RM500 rheometer equipped with a small gap Couette geometry (inner radius $r_1=10$ mm, outer radius $r_2=10.9$ mm). It can be noted that this gap was still sufficiently large to test cement suspensions which contain particles smaller than 100 μm. All surfaces in these measurement cells were covered with sand paper to prevent any slippage. Before each measurement, a pre-shearing phase at 150 s^{-1} was applied to

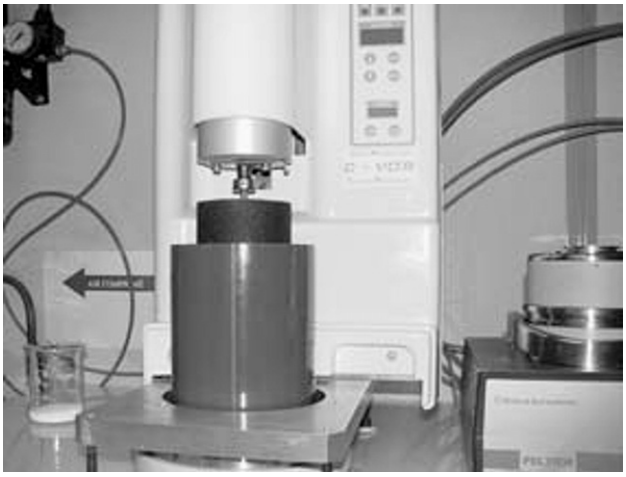

Fig. 1. Modified rheometer Bohlin C-VOR with the very large gap geometry used during MRI velocity measurements.

each sample for 60 s. Then, the imposed shear stress (imposed torque) on the sample was logarithmically varied every 10 s from 0.1 Pa to 150 Pa and then from 150 Pa to 0.1 Pa.

4. Results

4.1. Transient flow

The measured tangential velocity after an almost instantaneous decrease of the rotating velocity from 132 rpm to 51.5 rpm as a function of time for various radii inside the gap is plotted in Fig. 2. It can be seen that, close to the inner cylinder which imposes the rotating velocity to the material, tangential velocity is almost constant. However, as already demonstrated in [17], the evolution in time of the fluid velocity far from the inner cylinder displays two distinct successive trends.

In a first stage, there is a relatively rapid decrease of the tangential velocity. It has to be kept in mind that, before the measurement, the material was forced to flow at a much higher speed. When slowing down, its apparent viscosity increases and velocity decreases. The relative amplitude of this decrease increases with the distance from the inner cylinder. After a given time (of the order of 100 s), the velocity starts to increase again far from the inner cylinder.

We suggest the following interpretation of our data: over short timescales (our first stage) structural build-up and breakdown processes dominate, which lead to rapid thixotropic (reversible) effects, while over larger timescales non reversible phenomena such as hydration or chemical reactions between super-plasticizer molecules and cement particles [20] dominate, which lead to irreversible evolutions of the local behavior of the fluid. These two effects might in fact act at any time but, according to the above scheme, they appear to have very different characteristic times. As a consequence, it is reasonable to consider that there exists an intermediate period for which reversible effects have become negligible whereas irreversible effects have not yet become significant. This period corresponds to what we will define here as the "steady state" flow regime of the material. If the entire flow velocity profile inside the gap is considered, it is possible to define steady state as the state

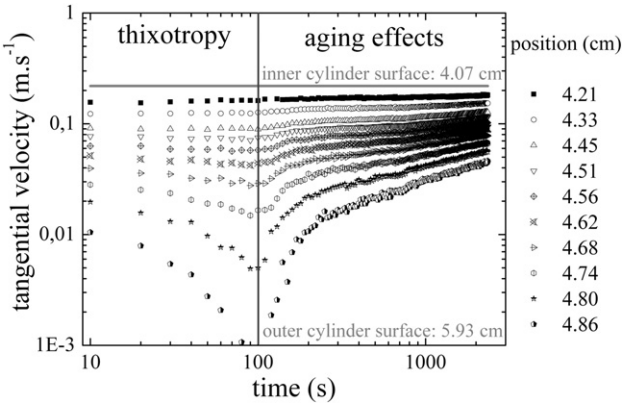

Fig. 2. Tangential velocity as a function of time at different radii inside the gap. A data point is recorded every 10 s. The inner cylinder rotating speed is 51.5 rpm. (Inner cylinder position 4.07 cm, outer cylinder 5.96 cm).

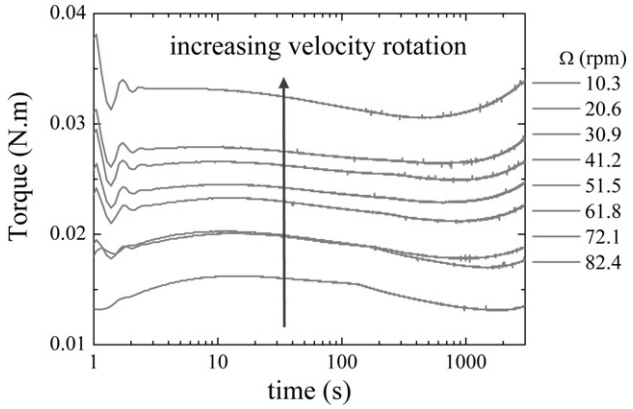

Fig. 3. Macroscopic torque as a function of time at different rotation speeds for the very large gap geometry used during the MRI measurements.

reached after 100 s for the rotation speed used to plot Fig. 2. The time needed to reach steady state varies between roughly 50 s at the highest rotation speed to almost 300 s at the lowest one.

It can however be noted that 100 s seem like a very short time compared to other results in literature. In most papers, a period of the order of magnitude of at least several thousand seconds is obtained from macroscopic and not local measurements, during which time irreversible hydration processes either do not seem to play a role or can be neglected. However, it can be noted that, as the material velocity increases at a given radius (Fig. 2) for an almost constant torque after the first hundreds of seconds (Fig. 3), this means that the apparent viscosity of the fluid is decreasing. This cannot be explained by hydration processes, which are expected to increase the apparent viscosity of the cementitious system with time. What is seen here could be explained by a delayed action of the super-plasticizer. This could be the case of the OPTIMA 100.

This phenomenon may in fact occur in any standard rheometer and not be spotted as its main effect (at least from a relative point of view) takes place far from the rotating cylinder (the inner one here). It has indeed to be kept in mind that the measured torque is only correlated to the shear rate, and thus shear stress, at the surface of the inner cylinder and that what happens far from the inner cylinder does not contribute directly to the measured torque. In the zone close to the inner cylinder where shear rates are high, no influence of the irreversible effects can be spotted before a couple of thousand seconds.

4.2. Steady flow

The velocity profiles (Fig. 4) exhibit two distinct regions: close to the inner cylinder, the paste is sheared and the velocity decreases almost linearly as a function of the radius. Close to the outer cylinder, the paste apparently does not flow. The interface between these two regions is situated at a critical distance r_c, which increases with the rotation speed of the inner cylinder Ω. This flow pattern in the case of cementitious materials had already been observed in [21,22]. Visual observations of a Couette flow indeed showed the same sheared and un-sheared zones. It is worth noting that the transition between these two regions seems somewhat abrupt: the slope of the velocity profile turns from a

finite, constant slope to almost zero, a phenomenon already observed with other thixotropic materials such as bentonite suspensions [17,18]. Although the authors do not specifically analyze this feature, it seems to also appear in the visual observations of the flow patterns in [21,22]. The existence of these two distinct zones is a known feature of yield stress materials but this breaking slope, as it will be shown in the next section, can not be predicted by any classical yield stress models such as Bingham or Herschel–Bulkley [16]. Indeed, these yield stress models predict a continuous transition between the two zones with the shear rate converging towards zero at the approach of the un-sheared zone. From these experimental results, we are able to determine the critical shear rate $\dot{\gamma}_c$, corresponding to the local slopes of the velocity profiles at the interface. This critical shear rate does not seem to depend on the flow boundary conditions and takes the average value of 9.5 s^{-1} for the cement paste studied in this work. The major consequence of the existence of this critical shear rate means that the material is not able to flow at shear rates below 9.5 s^{-1}. If one tries to use a small gap rheometer to apply to the material a shear rate lower than 9.5 s^{-1}, then, according to the above scheme, the gap will not be entirely sheared as the flow would have to localize in order to allow the material to flow with a shear rate higher than 9.5 s^{-1}. Moreover, torque measurements (cf. Fig. 3) were carried out with the Bohlin C-VOR rheometer with the same geometry as the MRI experiments. Tests were performed in exactly the same conditions in order to ensure the validity of the comparison. It can be noted that the initial fluctuations in Fig. 3 are due to inertia effects when the inner cylinder slow down from an initial rotating velocity of 132 rpm to the studied rotating velocity. From these torque measurements, we calculated the critical shear stress τ_c using Eq. (1) and the critical radii r_c directly obtained from velocity profiles. Its average value is 14.2 Pa for our cement paste and does not depend on the rotation speed or on the flow history. It can be noted that the fact that both critical shear rate and critical shear stress does not depend on boundary or initial conditions suggest that these are intrinsic rheological parameters of the fluid. Moreover, it can be seen in Fig. 2 that the irreversible evolution inside the gap although starting far from the inner cylinder after 100 s only affects the macroscopic torque after a couple of thousand seconds (Fig. 3), as found in other papers in literature.

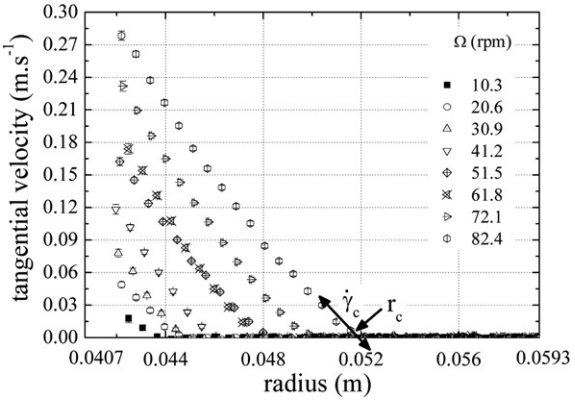

Fig. 4. Steady state tangential velocity as a function of radius inside the gap for various inner cylinder rotating speeds. Error bars for each measurement are also plotted.

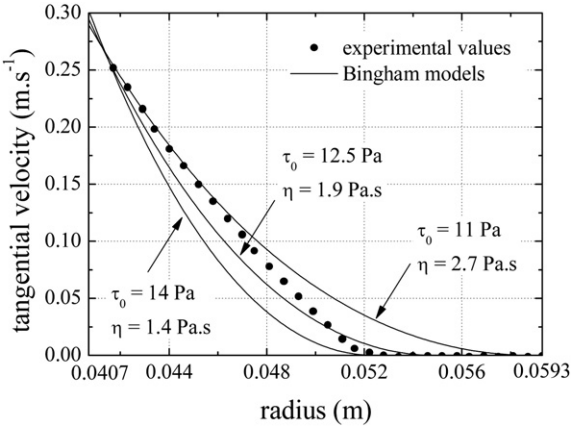

Fig. 5. Velocity as a function of radius inside the gap for a Couette flow for a 72.1 rpm rotating speed after 100 s. Continuous lines correspond to the predictions using various best fits of the Bingham model with different conditions: same unsheared thickness, similar slope in the sheared region, same overall shape.

4.3. Comparison with traditional models and the thixotropy model

4.3.1. Comparison with traditional models

We first consider the velocity profiles in steady state and try to fit a Bingham model to the measured local velocities. We choose to try to fulfill one of the following conditions: prediction and measurement display (i) the same unsheared thickness, (ii) a similar slope in the sheared region or (iii) the same overall shape. It can be noted from Fig. 5 that, no matter what value of the Bingham model parameters is used, the breaking slope cannot be predicted [17]. It was demonstrated in [17] that the same conclusions are reached if one tries to use a Herschel–Bulkley model. This could have been expected as demonstrated below. Eq. (3) can be written in the following form $\dot{\gamma} = |\partial v_\theta/\partial r - v_\theta/r|$. At the boundary between the sheared and un-sheared zones, no matter what model is used to describe the material behavior, the tangential velocity is equal to zero and the shear rate becomes $\dot{\gamma} = |\partial v_\theta/\partial r|$. This means that the slope of the velocity profile at the transition between the sheared

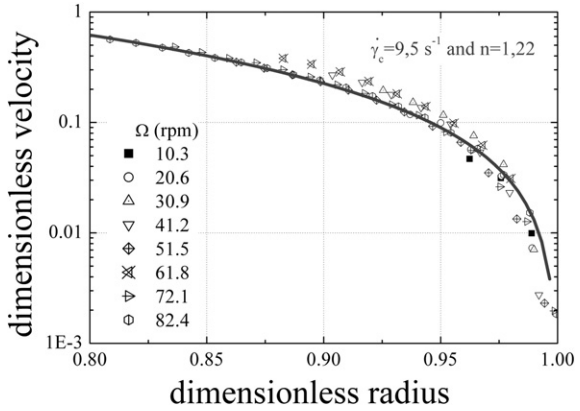

Fig. 6. Dimensionless master curve for steady state flow.

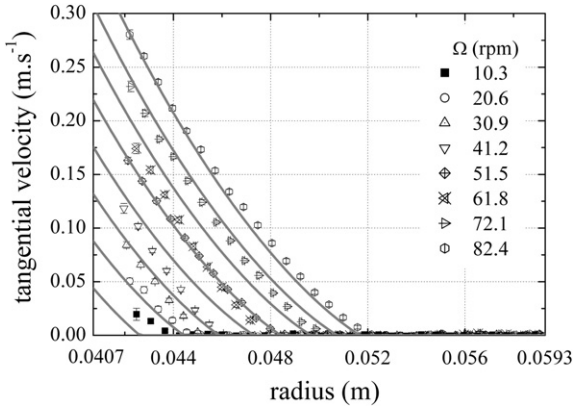

Fig. 7. Comparison between theoretical and experimental tangential velocity profiles for steady state flow.

and un-sheared zones is the shear rate itself. Traditional models predict that the shear rate at the boundary is equal to zero as the shear stress equals the yield stress at this radius (neither more nor less). The slope should then be horizontal at the boundary and the transition should be soft. This is not what we observe.

4.3.2. Comparison with a thixotropy model

From a practical point of view, it has been shown in [13] that it is very handy to plot the measured local velocities in the form of the dimensionless velocity V as a function of the dimensionless radius R with $V = v_\theta / r_c \dot{\gamma}_c$ and $R = r/r_c$ (cf. Fig. 6). It was moreover demonstrated in [13] that dimensionless velocity and extent of structure in the material λ may be derived from the following equations:

$$V(R) = \frac{n}{n-1} R \int_{R_1}^{1} \frac{R^{-3}}{1+\lambda^n(R)} dR \tag{10}$$

where $R_1 = r_1/r_c$ is the dimensionless radius of the inner cylinder.

$$\lambda^n(R) - k\frac{n}{n-1}\lambda(R) + 1 = 0. \tag{11}$$

Fitting these theoretical equations to the experimental data in Fig. 6 gives a value of $n = 1.22$. The viscosity $\eta_0 = 0.269$ Pa s is then calculated with the help of Eq. (9). The theoretical velocity profiles at steady state are then plotted in Fig. 7 and are in good agreement with the experimental measurements. More specifically, it can be noted that this model is able to predict the breaking slope.

The transient flow measurements allow for the fitting of the characteristic time of structural build-up in the material θ and consequently the parameter α with the help of Eq. (8). Theoretical predictions plotted in Fig. 8 are in good agreement with experimental measurements for the first 100 s (*i.e.* until the "steady state" flow we defined is reached). For longer observation times, the aging behavior becomes predominant far from the inner cylinder and the model predictions are of course not able to predict this non thixotropic evolution (*i.e.* irreversible).

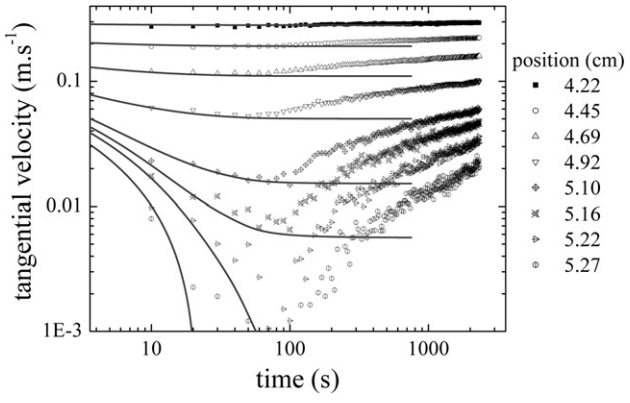

Fig. 8. Tangential velocity as a function of time at different radii inside the gap. Comparison between experimental measurements (symbols) and theoretical calculations (curves) for a rotation speed of 82.4 rpm.

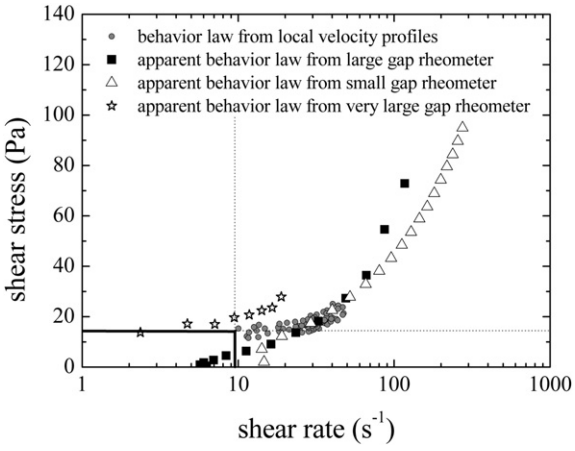

Fig. 9. Comparison between the local behavior law obtained from the MRI measurements and the apparent behavior laws obtained from standard rheometers.

4.4. Local behavior law

The measurements of the local tangential velocities and the associated macroscopic torque give access to the "local"

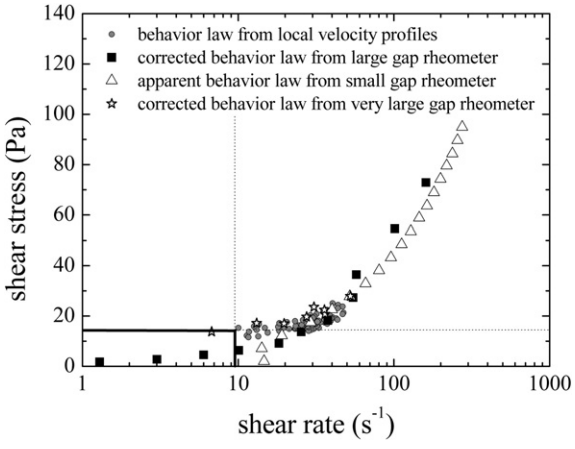

Fig. 10. Comparison between the local behavior law obtained from the MRI measurements and the corrected behavior laws obtained from standard rheometers.

behavior law of the material. This term designates a behavior law directly obtained from the analysis of the local velocity profiles and torque values without any assumption on the shear stress and/or shear rate distribution within the gap in opposition with "apparent" rheograms obtained from macroscopic measurements with rheometers. Torque measurements associated with Eq. (2) give access to the shear stress distribution whereas velocity profiles with Eq. (3) allows for the determination of the shear rate distribution.

By plotting the local shear stress as a function of the local shear rate, we obtained the behavior law plotted in Fig. 9 which can be considered as the reference behavior law for our material. One can observe that the critical shear stress and shear rate define an area where no local data can be found as the material is not able to flow at stresses lower than the critical shear stress or at shear rates lower than the critical shear rate.

Let us now compare with the apparent behavior laws obtained with standard rheometers using the apparent shear rates and shear stress defined in Section 2. It can be seen that the small gap rheometer gives the same behavior law in the shear rate range studied in the MRI local velocity measurements. This means that the assumption of a small gap is valid and that this type of measurement is suitable for cementitious materials as long as the shear stress and shear rate are higher than the critical values. It can indeed be seen that, if one tries to extrapolate the yield stress from the behavior law obtained with the small gap rheometer, the yield stress value obtained will be far lower than the real one.

It can also be noted that there is a strong difference between the local behavior law and the behavior laws obtained with the large gap rheometers especially in the case of the very large gap geometry. The calculation of the apparent shear rate in the case of these incompletely sheared gaps induces a strong deviation from the real behavior of the material. Moreover, it can be noted that some data can be found in the zone where the material is not supposed to be able to flow.

We now use the reconstruction method based on the torque (C) and rotation speed (Ω)developed by Nguyen and Boger [23] in the case where the gap is not entirely sheared

$$\dot{\gamma}(\tau(r_i)) = 2C\frac{d\Omega}{dC} = 2\Omega\frac{d\ln\Omega}{d\ln C}. \quad (12)$$

The application of this method leads to the corrected behavior laws plotted in Fig. 10. All the data obtained are now superimposed with the reference behavior law of the tested material. This means that, even when using a large gap rheometer, it is possible to correct the calculated apparent shear rate by using, for example, the Nguyen and Boger method and thus have access to the real rheological parameters of the tested material.

However, it has to be kept in mind that, even when corrected with the above method, the data obtained for the lowest values of the shear rates or shear stresses (lower than the critical values of the shear rate and stress) could lead to extrapolated values of the yield stress which are lower than the real ones.

5. Conclusion

In the first section, the main features of Couette flow viscometers were reviewed and a simple thixotropy model was described. Experimental results obtained from MRI measurements and from standard rheometry tests were then presented and analyzed. It was then shown that classical yield stress models were not able to predict the measured local velocity field whereas the predictions of the simple thixotropy model used here were in good agreement with our measurements. Finally, the local (or real) behavior law of the studied cement paste was deduced from the local MRI measurements and compared to the apparent behavior law calculated from standard rheometric measurements. It was finally demonstrated that it is possible to use correction techniques from the literature to have access to the real behavior law of the material from these standard measurements but that, in the case of the material studied in this paper, this would nevertheless lead to an underestimation of the yield stress.

References

[1] C. Atzeni, L. Massidda, U. Sanna, Comparison between rheological models for Portland cement pastes, Cem. Concr. Res. 15 (1985) 511–519.
[2] A. Yahia, K.H. Khayat, Analytical model for estimating yield stress of high performance pseudo-plastic grout, Cem. Concr. Res. 31 (2001) 731–738.
[3] Y. Otsubo, S. Miyai, K. Umeya, Time-dependent flow of cement pastes, Cem. Concr. Res. 10 (1980) 631–638.
[4] P.F.G. Banfill, D.C. Saunders, On the viscometric examination of cement pastes, Cem. Concr. Res. 11 (1981) 363–370.
[5] R. Lapasin, A. Papo, S. Rajgelj, Flow behaviour of cement pastes. A comparison of different rheological instruments and techniques, Cem. Concr. Res. 13 (1983) 349–356.
[6] G.H. Tattersall, The rheology of Portland cement pastes, Br. J. Appl. Phys. 6 (1955) 165–167.
[7] A. Papo, The thixotropic behavior of white Portland cement pastes, Cem. Concr. Res. 18 (1988) 595–603.
[8] J.E. Wallevik, Thixotropic investigation on cement paste: experimental and numerical approach, J. Non-Newton. Fluid Mech. 132 (2005) 86–99.
[9] P. Coussot, J.S. Raynaud, F. Bertrand, P. Moucheronr, J.P. Guilbaud, H.T. Huynh, S. Jarny, D. Lesueur, Coexistence of liquid and solid phases in flowing soft-glassy materials, Phys. Rev. Lett. 88 (2002) 218301 4 pages.
[10] A.J. Liu, S.R. Nagel, Jamming is not cool any more, Nature 21 (1998) 396–397.
[11] D.H. Cheng, F. Evans, Phenomenological characterization of the rheological behaviour of inelastic reversible thixotropic and antithixotropic fluids, Br. J. Appl. Phys. 16 (1965) 1599.
[12] P. Coussot, Q.D. Nguyen, H.T. Huynh, D. Bonn, Viscosity bifurcation in thixotropic, yielding fluids, J. Rheol. 46 (3) (2002) 573–589.
[13] N. Roussel, R. Le Roy, P. Coussot, Thixotropy modelling at local and macroscopic scales, J. Non-Newton. Fluid Mech. 117 (2004) 85–95.
[14] N. Roussel, Steady and transient flow behaviour of fresh cement pastes, Cem. Concr. Res. 35 (2005) 1656–1664.
[15] N. Roussel, A thixotropy model for fresh fluid concretes: theory, validation and applications, Cem. Concr. Res. 36 (10) (2006) 1797–1806.
[16] R. Shaughnessy, P.E. Clark, The rheological behaviour of fresh cement pastes, Cem. Concr. Res. 18 (1988) 327–341.
[17] S. Jarny, N. Roussel, S. Rodts, F. Bertrand, R. Le Roy, P. Coussot, Rheological behavior of cement pastes from MRI velocimetry, Cem. Concr. Res. 35 (2005) 1873–1881.

[18] A.D. Hanlon, S.J. Gibbs, L.D. Hall, D.E. Haycock, W.J. Frith, S. Ablett, Rapid MRI and velocimetry of cylindrical Couette flow, Magn. Reson. Imaging 16 (8) (1998) 953–961.
[19] J.S. Raynaud, P. Moucheront, J.C. Baudez, F. Bertrand, J.P. Guilbaud, P. Coussot, Direct determination by NMR of the thixotropic and yielding behavior of suspensions, J. Rheol. 46 (2002) 709–732.
[20] R.J. Flatt, Y.F. Houst, A simplified view on chemical effects perturbing the action of superplasticizers, Cem. Concr. Res. 31 (8) (2001) 1169–1176.
[21] C.R. Dimond, The rheology of cement pastes, PhD thesis, University of Sheffield, 1975.
[22] G.H. Tatersall, P.G.F. Banfill, The Rheology of Fresh Concrete, Pitman, London, 1983.
[23] Q.D. Nguyen, D.V. Boger, Characterization of yield stress fluids with concentric cylinder viscometers, J. Rheol. 26 (1987) 508–515.